Electric quadrupole transitions in carbon dioxide

Andrey Yachmenev, Alain Campargue, Sergei N Yurchenko, Jochen Küpper,
Jonathan Tennyson

Electric quadrupole transitions in carbon dioxide

Andrey Yachmenev,[1, 2, *] Alain Campargue,[3, †] Sergei N. Yurchenko,[4, ‡] Jochen Küpper,[1, 2, 5] and Jonathan Tennyson[4]

[1] Center for Free-Electron Laser Science, Deutsches Elektronen-Synchrotron DESY, Notkestraße 85, 22607 Hamburg, Germany
[2] Center for Ultrafast Imaging, Universität Hamburg, Luruper Chaussee 149, 22761 Hamburg, Germany
[3] Univ. Grenoble Alpes, CNRS, LIPhy, 38000 Grenoble, France
[4] Department of Physics and Astronomy, University College London, London, WC1E 6BT, UK
[5] Department of Physics, Universität Hamburg, Luruper Chaussee 149, 22761 Hamburg, Germany
(Dated: January 26, 2021)

Recent advances in the high sensitivity spectroscopy have made it possible, in combination with accurate theoretical predictions, to observe for the first time very weak electric quadrupole transitions in a polar polyatomic molecule of water. Here we present accurate theoretical predictions of the complete quadrupole ro-vibrational spectrum of a non-polar molecule CO_2, important in atmospheric and astrophysical applications. Our predictions are validated by recent cavity enhanced absorption spectroscopy measurements and are used to assign few weak features in the recent ExoMars ACS MIR spectroscopic observations of the martian atmosphere. Predicted quadrupole transitions appear in some of the mid-infrared CO_2 and water vapor transparency regions, making them important for detection and characterization of the minor absorbers in water- and CO_2-rich environments, such as present in the atmospheres of Earth, Venus and Mars.

The intensities of electric quadrupole (E2) transitions are known to be very weak, six to eight orders of magnitude smaller than the intensities of electric dipole (E1) transitions. Until very recently, the E2 transitions were measured only in non-polar or slightly polar diatomics, such as H_2 [1–6], O_2, N_2 [7–11], HD [12], N_2^+ [13], i.e., molecules that otherwise do not exhibit E1 transitions or, as regards HD, they are extremely weak. In polar molecules, with polyatomics being considerably richer in the number and density of ro-vibrational transitions, strong E1 absorption profiles blanket most of the weak features in the ro-vibrational spectrum. Tracing and assigning weak spectral features as belonging to the E1 transitions of minor isotopologues or other meager molecular species or indeed rather the E2 or magnetic dipole (M1) transitions of the main molecular constituent, can be endlessly intricate and hence quite often demand precise theoretical predictions. So far as there were no reliable calculations of the E2 and magnetic dipole M1 transitions for polyatomic molecules, detection of these dipole-forbidden features and investigation of their seemingly surreptitious role in high-resolution spectroscopy remains unexplored.

The role of weak ro-vibrational transitions in spectrum of carbon dioxide (CO_2) is fundamental to monitoring its isotopic composition in the atmosphere for understanding of carbon cycle processes [14–17] and it is becoming increasingly precise for determination of new gas signatures in CO_2-rich planetary atmospheres, such as Mars and Venus. For this purposes, the completeness of spectroscopic data for the main isotopologue $^{12}C^{16}O_2$ is crucial, especially in its transparency windows, to reduce the likelihood of deceiving its weak spectroscopic features for minor isotopologues or other less abundant molecular species [18, 19]. For example, recently discovered weak M1 transitions of CO_2 in the spectrum of the martian at-

mosphere [19] would not be known as belonging to CO_2 without the accurate knowledge of the E1 transitions of its main and minor isotopologues. While there have been multiple and still ongoing computational and experimental efforts to fully characterize the E1 spectra of major isotopologues of CO_2 [20–22], the contributions from the dipole-forbidden E2 and, until very recently M1 [19], transitions have not had the slightest attention.

In this letter, we report the first complete and accurate E2 line list for carbon dioxide $^{12}C^{16}O_2$, which was validated in the 3.3 μm transparency window by recent laboratory measurements using Optical-Feedback-Cavity Enhanced Absorption Spectroscopy (OFCEAS) [23]. Based on our predictions and laboratory measurements, we report a detection of the E2 lines in the martian atmospheric spectra recorded by the ExoMars Trace Gas Orbiter Atmospheric Chemistry Suite (ACS) instrument [24]. We also present our newly developed variational computational methodology, which is capable of high-accuracy predictions of the E2 spectra for arbitrary polar molecules.

Our computational approach is based on the general variational approach TROVE [25–28], which for triatomic molecules employs exact kinetic energy operator [29]. For CO_2, an accurate empirically refined potential energy surface (PES) 'Ames-2' was employed [30]. In TROVE, the vibrational basis set is constructed in a multi-step procedure from contracted and symmetry-adapted products of one-dimensional basis sets, each represented by solutions $\chi_n(q)$ ($n = 0, 1, 2...$) of one-dimensional Schrödinger equation for a selected vibrational mode q [27]. For CO_2 there are two stretching and one bending vibrational modes, with the respective quantum numbers n_1, n_2, n_3. Since CO_2 is linear, its bending vibration is coupled to a molecular rotational motion about the linearity axis, which is the molecular z

axis. For this reason, the bending basis functions cannot be fully decoupled from the molecular rotation and parametrically depend on the rotational quantum number K of the $\hat{J}_z$ angular momentum operator, hence the notation $n_3^{(K)}$. We refer for details of treatment of linear and quasi-linear molecules to [29]. The size of vibrational basis was controlled by a condition $2(n_1 + n_2) + n_3^{(K)} \leq 64$.

The full ro-vibrational basis set is constructed as a symmetrized product of the symmetry-adapted vibrational basis functions $\psi_{\lambda,K}^{(\Gamma_{\text{vib}})}$ and symmetry-adapted rigid-rotor wave functions $|J, K, \Gamma_{\text{rot}}\rangle$:

$$\Psi_{\lambda,K}^{(J,\Gamma)} = \{\psi_{\lambda,K}^{(\Gamma_{\text{vib}})} \times |J, K, \Gamma_{\text{rot}}\rangle\}^{\Gamma}. \quad (1)$$

Here, λ denotes a set of vibraitonal state quantum numbers, and Γ_{vib}, Γ_{rot}, and Γ denote the symmetries of the vibrational, rotational and total wave functions, respectively. For CO_2 we employed the $\mathbf{C}_{2v}(M)$ molecular symmetry group. The total wavefunction for a ro-vibrational state l, with the quantum number of the total angular momentum J and the total symmetry Γ, is a linear combination of ro-vibrational basis set functions:

$$\Phi_l^{(J,\Gamma)} = \sum_{K,\lambda} c_{K,\lambda}^{(J,\Gamma,l)} \Psi_{\lambda,K}^{(J,\Gamma)}, \quad (2)$$

where the linear expansion coefficients $c_{K,\lambda}^{(J,\Gamma,l)}$ are obtained by solving an eigenvalue problem with the full ro-vibrational Hamiltonian. All energies and eigenfunctions up to $J = 40$ were generated and used to produce the E2 line list for CO_2.

The achieved accuracy of energy level predictions for CO_2 is best characterized by the root-mean-squares (rms) deviation of 0.06 cm^{-1} between the calculated and experimental [31] ro-vibrational term values, evaluated across 337 band centers with energies up to $15\,500$ cm^{-1} above zero-point level. Considering the weakness of the E2 lines, the line position accuracy is crucial for discriminating them from the weak E1 lines of minor isotopologues and possible impurities. Further improvement of accuracy would require yet another round of empirical adjustment of the underlying PES, which is an inordinately expensive procedure. As a call for more practical solution very often the variationally computed energies, providing they are close enough to experiment, are replaced by the corresponding experimentally determined values. The latter can be extracted from the experimental spectroscopic line positions using advanced combination difference techniques such as, for example, MARVEL (Measured Active Rotational-Vibrational Energy Levels) [32–35] and RITZ (Rydberg-Ritz combination principle) [36, 37]. For CO_2, we used the experimental energy levels from the Carbon Dioxide Spectroscopic Databank [38] produced from a global effective Hamiltonian modeling of an exhaustive set of position measurements available in the literature [39]. More details about

employed here computational procedure and validation of its accuracy are presented in a study of the E1 line list of CO_2 [22].

The quadrupole spectrum was simulated using the variational approach RichMol [40, 41], a computer program designed for calculations of molecular ro-vibrational dynamics in the presence of external electromagnetic field. The transition probability from an initial ro-vibrational state $|i\rangle = \Phi_l^{(J,\Gamma)}$ into a final state $|f\rangle = \Phi_{l'}^{(J',\Gamma')}$ due to the interaction of light with quadrupole moment of molecule is given by

$$P(f \leftarrow i) = g_{\text{ns}}(2J' + 1)(2J + 1)\left|\mathcal{K}^{(J',\Gamma',l',J,\Gamma,l)}\right|^2 \quad (3)$$

where

$$\mathcal{K}^{(J',\Gamma',l',J,\Gamma,l)} = \sum_{K'\lambda'} \sum_{K\lambda} \left[c_{K',\lambda'}^{(J',\Gamma',l')}\right]^* c_{K,\lambda}^{(J,\Gamma,l)} \quad (4)$$

$$\times (-1)^{K'} \sum_{\sigma=-2}^{2} \begin{pmatrix} J & 2 & J' \\ K & \sigma & -K' \end{pmatrix}$$

$$\times \sum_{\alpha,\beta=x,y,z} U_{\sigma,\alpha\beta}\langle\psi_{\lambda',K'}|Q_{\alpha,\beta}|\psi_{\lambda,K}\rangle.$$

Here, $Q_{\alpha,\beta}$ denotes the traceless quadrupole moment tensor in the molecular frame and the matrix $U_{\sigma,\alpha\beta}$ transforms quadrupole tensor from Cartesian to spherical-tensor form (see, e.g., Eqs. (5-41)–(5-44) in [42]). The nuclear spin statistical factors g_{ns} for $^{12}C^{16}O_2$ are equal to one for initial state symmetries A_1 and A_2 and zero otherwise.

The quadrupole moment tensor with elements as functions of internal coordinates is required to compute the vibrational expectation values $\langle\psi_{\lambda',K'}|Q_{\alpha,\beta}|\psi_{\lambda,K}\rangle$ in Eq. (4). A three-dimensional mesh of internal coordinates of CO_2 was used, containing about 2000 different nuclear geometries and covering the energy range up to $hc\cdot40\,000$ cm^{-1} above the equilibrium energy. The quadrupole tensor at each point was computed using all-electron CCSD(T) level of theory in conjunction with the aug-cc-pwCVQZ basis set [43–45] and analytic gradient approach [46]. The electronic structure calculations employed the quantum chemistry package CFOUR [47]. For a molecular frame selected such that the x axis bisects the valence bond angle O–C–O and plane of the molecule for bent CO_2 is aligned with the xz plane, the three nonzero elements of the quadrupole tensor Q_{xx}, Q_{zz} and Q_{xz} have the A_1, A_1, and B_2 symmetries, respectively. These were parameterized using fourth order symmetry-adapted power series expansions through least-squares fittings to the electronic structure data, with $\sigma_{\text{rms}} < 10^{-4}$ a.u.

Our results for the quadrupole moment of CO_2 $Q_{zz}^{\text{e}} = -3.1666$ a.u. $= -14.207 \times 10^{-40}$ Cm^2 at the equilibrium $r_e = 1.1614$ Å and its zero-point vibrational average $Q_{zz}^{\text{ZPVA}} = -3.1627$ a.u. $= -14.190 \times 10^{-40}$ Cm^2

TABLE I. Experimental and theoretical permanent electric quadrupole moments of CO_2 in 10^{-40} Cm^2

Method	Value	Source
Experiment		
Buckingham effect[a]	-14.98 ± 0.50	[48]
Buckingham effect[a]	-14.3 ± 0.6	[49]
Buckingham effect[a]	-14.31 ± 0.74	[50]
Cotton-Mouton effect[b]	-14.0 ± 0.7	[51]
Collision-induced absorption	-14.9 ± 0.7	[52]
Dielectric measurements	-14.94 ± 1.0	[53]
Theory		
CCSD(T)/CBS[c]	-14.22 ± 0.09	[54]
CCSD(T)/CBS + ZPVC[d]	-14.29 ± 0.09	[54]
CCSD(T)/6s4p4d1f	-14.3	[55]
CCSD(T)/AwCVQZ	-14.207	This work
CCSD(T)/AwCVQZ/ZPVC[d]	-14.190	This work

[a] Electric field gradient induced birefringence measurements.
[b] Magnetic field induced birefringence measurements.
[c] Complete basis set limit extrapolation with additive core-valence correlation effect.
[d] Results corrected with the zero-point vibration.

agree very well with experimental data and previous calculations listed in Table I.

The integrated absorption coefficient of quadrupole transition in units cm/molecule is given by

$$I(f \leftarrow i) = \frac{4\pi^5 \nu^3 e^{-\beta E_l^{(J,\Gamma)}} \left(1 - e^{-\beta h c \nu}\right)}{(4\pi\epsilon_0) 5 h c Z(T)} P(f \leftarrow i), \quad (5)$$

where $\nu = (E_{l'}^{(J',\Gamma')} - E_l^{(J,\Gamma)})/hc$ is the frequency of transition between lower $E_l^{(J,\Gamma)}$ and upper $E_{l'}^{(J',\Gamma')}$ state energies, $Z(T)$ is the partition function, and $\beta = 1/(kT)$. For $^{12}C^{16}O_2$ we used an accurate computed value of $Z(296 \text{ K}) = 286.094$ [20]. The computed quadrupole line list is provided as supplementary material to the paper.

On the upper panel of Fig. 1, the calculated E2 line list for the main isotopologue, $^{12}C^{16}O_2$, is superimposed on the E1 line list of the natural CO_2 [31]. Both spectra are generated at room temperature, $T = 296$ K. The E1 lines of the minor isotopologues at natural abundances are plotted on the figure with cyan color. In general, the E2 bands are 6–8 orders of magnitude weaker than the E1 bands. The most prominent E2 band with the line intensities of a few 10^{-29} cm/molecule is the bending plus anti-symmetric stretching $\nu_2 + \nu_3$ band at 3000 cm^{-1} (3.3 μm), shown on the lower panel of Fig. 1.

In contrast with E2 spectrum of water [56, 57], the E2 lines of CO_2 appear largely in the E1 transparency regions, which makes them possible to observe, and perhaps most important, they may thereby play an essential role in detections of minor isotopologues and small amounts of other gases in CO_2-rich environments. The reason for this is different approximate selection rules for
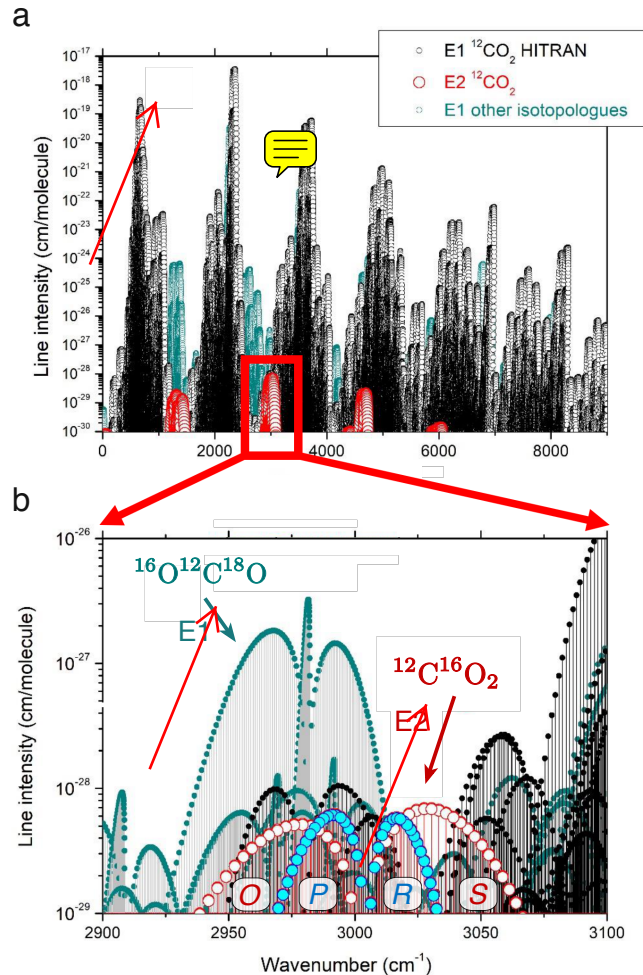

FIG. 1. (a) Overview of the calculated quadrupole spectrum of $^{12}C^{16}O_2$(red) superimposed with its dipole spectrum (black) and the dipole spectrum of minor isotopologues (cyan). The spectra are generated for temperature $T = 296$ K. (b) A zoom into the $\nu_2 + \nu_3$ band, where the E2 transitions of $^{12}C^{16}O_2$ can be distinguished by larger circles, the P and R branches plotted with cyan colour and O and S branches plotted with red colour.

the E1 and E2 transitions in CO_2 and in linear molecules in general. For example, the ν_2 and $\nu_2 + \nu_3$ E1 band transitions at 6.9 and 3.3 μm are dipole forbidden and therefore very weak. These bands are however directly allowed for the E2 transition mechanism, even in the rigid-rotor approximation.

As already mentioned, the E1 lines of the minor isotopologues of CO_2 make an important contribution to the transparency windows (see Fig. 1), where they overlap with the E2 lines of the main isotopologue. Indeed, the predicted $\nu_2 + \nu_3$ E2 band of $^{12}C^{16}O_2$ is almost entirely superimposed with the $\nu_2 + \nu_3$ E1 band of $^{16}O^{12}C^{18}O$, which is stronger by about a factor 20, in spite a natural isotopic abundance of only 4×10^{-3}. It should be noted that due to the different symmetry, the $\nu_2 + \nu_3$ E1 band
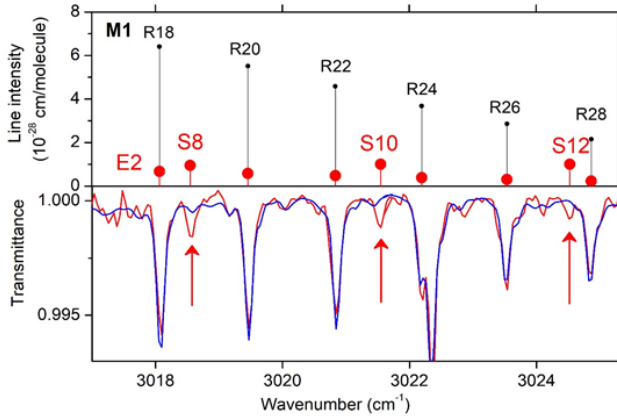
FIG. 2. Comparison of the ACS MIR transmission spectra of the atmosphere of Mars [19] near 3020 cm^{-1} with calculated line lists of the M1 and E2 $\nu_2 + \nu_3$ bands of ^{12}C^{16}O$_2$. Upper panel: The presently calculated E2 transitions with *ab initio* intensities (red stems) are superimposed to the M1 transitions with intensities ~~measured in [19]~~ (black stems). Lower panel: ACS MIR spectrum (red line) with a best-fit synthetic model containing the contributions of the E1 bands of CO$_2$ and H$_2$O based on HITRAN 2016 database and of the M1 lines identified in [19]. The assignments of the newly detected S8~~ S12~~ E2 transitions are marked with red arrows.

is allowed in ^{16}O^{12}C^{18}O but forbidden in ^{12}C^{16}O$_2$.

The $\nu_2 + \nu_3$ band of CO$_2$ has recently been observed in the spectrum of Mars' atmosphere [19], as recorded by the ExoMars Trace Gas Orbiter ACS-MIR (Atmospheric Chemistry Suite Mid InfraRed) spectrometer. The recorded spectra show strong intensity features that are more specific for the M1 rather than the E2 transitions, although no first principles simulations for the M1 spectrum had been done. In particular, the presence of the strong Q-branch, which is very weak for the E2 band, see Fig. 1.b, and the absence of nearly as intense the O- and S-branches argue for a dominant M1 mechanism. But this does not exclude presence of the E2 features in the martian spectrum, although obviously they must be less pronounced.

As can be seen from Fig. 1.b, E2 transitions in the O-branch overlap completely with much stronger and generally broader E1 lines of CO$_2$, hence hardly discernible. A number of the S-branch transitions appear in a narrow region free from any strong E1 lines, which are thus possible to observe. In Fig. 2, we compare the predicted S-branch transitions near 3020 cm^{-1} to the ACS MIR transmission spectra displayed on Fig. 4 of [19]. A clear position coincidence of the predicted $S(8)$, $S(10)$ and $S(12)$ lines with unknown weak absorption features can be observed in the region 3018–3025 cm^{-1}.

A very recent laboratory study, dedicated to measurements of the weak spectral features in the S-branch of $\nu_2 + \nu_3$ band of CO$_2$ by OFCEAS [23], has confirmed the

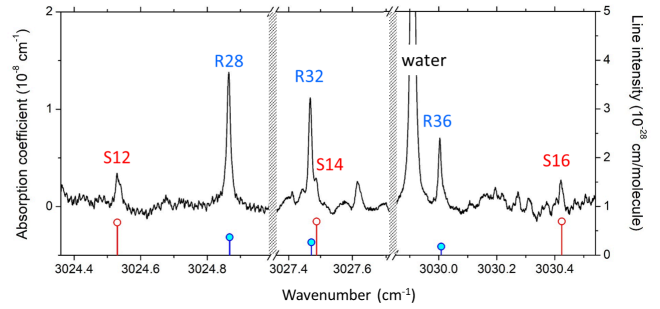FIG. 3. Comparison of the laboratory spectrum of CO$_2$ at 60 mbar recorded by OFCEAS [23] with the calculated E2 line list of ^{12}C^{16}O$_2$ in three spectral intervals of the E2 $\nu_2 + \nu_3$ band. The R- and S-band transitions are plotted with blue and red stems, respectively. The S12, S14 and S16 E2 lines are apparent. The line intensities of the R28, R32 and R36 transitions is mostly due to the M1 transitions.

strong M1 features originally observed in ~~m~~artian CO$_2$. The measurement have also revealed a number of new features that can be assigned, by comparison with theoretical line list, to the S12, S14, and S16 E2 lines, shown in Fig. 3. Notably, the E2 R-branch transitions provide about 10–15% intensity of the dominant M1 features.

~~Intensity considerations provide further evidence supporting the detection of E2 lines in ACS MIR spectrum. The absolute intensities of M1 transitions detected in [19] (also shown in Fig. 2) were derived by a scaling to the adjacent $\nu_2 + \nu_3$ E1 band of ^{16}O^{12}C^{18}O with well known absolute line intensities. The resulting intensity values for M1 transitions are in the range between 6.9 and 4.3$\times 10^{-28}$ cm/molecule for an ACS MIR temperature of 172 K. By scaling the newly assigned E2 transmittance dips to the once of M1 type, the absolute experimental intensities of S8, S10, and S12 transitions can be estimated at about 1 $\times 10^{-28}$ cm/molecule, which is in excellent agreement with our theoretically predicted values for S(8)–S(12) of 9.4$\times 10^{-29}$, 9.9$\times 10^{-29}$, 9.9$\times 10^{-29}$ cm/molecule, respectively~~

In summary, we presented an accurate computational methodology for calculating the electric quadrupole spectra of polyatomic molecules with arbitrary structure. Calculated quadrupole transitions of CO$_2$ were confirmed by the high sensitivity spectroscopic measurements [23] with few of them newly identified in the spectrum of Mars' atmosphere. The quadrupole transitions are typically a million times weaker than the electric dipole transitions, thus comparable in strength to the dipole transitions of the absorbers at a low relative abundance, such as, for example, minor isotopologues. The accurate characterization of the quadrupole transitions for the main atmospheric absorbers, especially in the mid-infrared transparency windows, will eliminate the misassignment of spectral features and thus help in precise detection of the minor atmospheric constituents. Being particularly

sensitive to steeply varying fields, which are common in nature at the molecule-molecule and molecule-surface interfaces [58–60], the electric quadrupole transitions can potentially be used for remote sensing of local molecular environments.

---

* andrey.yachmenev@cfel.de
† alain.campargue@univ-grenoble-alpes.fr
‡ s.yurchenko@ucl.ac.uk

[1] G. Herzberg, Quadrupole Rotation-Vibration Spectrum of the Hydrogen Molecule, Nature **163**, 170 (1949).

[2] A. Goldman, J. Reid, and L. S. Rothman, Identification of electric quadrupole O_2 and N_2 lines in the infrared atmospheric absorption spectrum due to the vibration-rotation fundamentals, Geophys. Res. Lett. **8**, 77 (1981).

[3] D. Reuter, D. Jennings, and J. Brault, The $v = 1 \leftarrow 0$ quadrupole spectrum of N_2, J. Mol. Spectrosc. **115**, 294 (1986).

[4] K. H. Baines, M. E. Mickelson, L. E. Larson, and D. W. Ferguson, The abundances of methane and ortho/para hydrogen on uranus and neptune: Implications of new laboratory 4-0 h2 quadrupole line parameters, Icarus **114**, 328 (1995).

[5] A. Campargue, S. Kassi, K. Pachucki, and J. Komasa, The absorption spectrum of H_2: CRDS measurements of the (2-0) band, review of the literature data and accurate ab initio line list up to 35000 cm^{-1}, Phys. Chem. Chem. Phys. **14**, 802 (2012).

[6] S.-M. Hu, H. Pan, C.-F. Cheng, Y. R. Sun, X.-F. Li, J. Wang, A. Campargue, and A.-W. Liu, The $v = 3 \leftarrow 0$ $S(0)$–$S(3)$ Electric Quadrupole Transitions of H_2 near 0.8 μm, Astrophys. J. **749**, 76 (2012).

[7] J. Reid, R. L. Sinclair, A. M. Robinson, and A. R. W. McKellar, Observation of electric quadrupole transitions in the fundamental band of o2 in the 1600-cm^{-1} region, Phys. Rev. A **24**, 1944 (1981).

[8] L. S. Rothman and A. Goldman, Infrared electric quadrupole transitions of atmospheric oxygen, Appl. Optics **20**, 2182 (1981).

[9] S. Kassi and A. Campargue, Cavity ring down spectroscopy with 5×10^{-13} cm^{-1} sensitivity, J. Chem. Phys. **137**, 234201 (2012).

[10] S. Kassi, I. E. Gordon, and A. Campargue, First detection of transitions in the second quadrupole overtone band of nitrogen near 1.44 μm by CW-CRDS with 6×10^{-13} cm^{-1} sensitivity, Chem. Phys. Lett. **582**, 6 (2013).

[11] P. Čermák, S. Vasilchenko, D. Mondelain, S. Kassi, and A. Campargue, First laboratory detection of an absorption line of the first overtone electric quadrupolar band of N_2 by CRDS near 2.2 μm, Chem. Phys. Lett. **668**, 90 (2017).

[12] S. Vasilchenko, D. Mondelain, S. Kassi, P. Čermák, B. Chomet, A. Garnache, S. Denet, V. Lecocq, and A. Campargue, The HD spectrum near 2.3 μm by CRDS-VECSEL: Electric quadrupole transition and collision-induced absorption, J. Mol. Spectrosc. **326**, 9 (2016).

[13] M. Germann, X. Tong, and S. Willitsch, Observation of electric-dipole-forbidden infrared transitions in cold molecular ions, Nature Physics **10**, 820 (2014).

[14] W. G. Mook, M. Koopmans, A. F. Carter, and C. D. Keeling, Seasonal, latitudinal, and secular variations in the abundance and isotopic ratios of atmospheric carbon dioxide: 1. results from land stations, J. Geophys. Res.: Ocean **88**, 10915 (1983), https://agupubs.onlinelibrary.wiley.com/doi/pdf/10.1029/JC088i

[15] E. Kerstel and H. Meijer, Optical isotope ratio measurements in hydrology, in *Isotopes in the Water Cycle: Past, Present and Future of a Developing Science*, edited by P. K. Aggarwal, J. R. Gat, and K. F. Froehlich (Springer Netherlands, Dordrecht, 2005) pp. 109–123.

[16] H. D. Graven, Impact of fossil fuel emissions on atmospheric radiocarbon and various applications of radiocarbon over this century, Proc. Nat. Acad. Sci. **112**, 9542 (2015), https://www.pnas.org/content/112/31/9542.full.pdf.

[17] J. Lelieveld, K. Klingmüller, A. Pozzer, R. T. Burnett, A. Haines, and V. Ramanathan, Effects of fossil fuel and total anthropogenic emission removal on public health and climate, Proc. Nat. Acad. Sci. **116**, 7192 (2019), https://www.pnas.org/content/116/15/7192.full.pdf.

[18] A. D. McCartt, T. Ognibene, G. Bench, and K. Turteltaub, Measurements of carbon-14 with cavity ring-down spectroscopy, Nuclear Instruments and Methods in Physics Research Section B: Beam Interactions with Materials and Atoms **361**, 277 (2015).

[19] A. Trokhimovskiy, V. Perevalov, O. Korablev, A. Fedorova, K. Olsen, J. Bertaux, A. Patrakeev, A. Shakun, F. Montmessin, F. Lefèvre, and L. A., First observation of the magnetic dipole CO2 main isotopologue absorption band at 3.3 μm in the atmosphere of Mars by the ExoMars Trace Gas Orbiter ACS instrument, Astron. Astrophys. **639**, A142 (2020).

[20] E. J. Zak, J. Tennyson, O. L. Polyansky, L. Lodi, N. F. Zobov, S. A. Tashkun, and V. I. Perevalov, Room temperature line lists for CO_2 asymmetric isotopologues with *ab initio* computed intensities, J. Quant. Spectrosc. Radiat. Transf. **203**, 265 (2017).

[21] T. Odintsova, E. Fasci, L. Moretti, E. J. Zak, O. L.

Polyansky, J. Tennyson, L. Gianfrani, and A. Castrillo, Highly-accurate intensity factors of pure co$_2$ lines near 2 μm, J. Chem. Phys. **146**, 244309 (2017).

[22] S. N. Yurchenko, T. M. Mellor, R. S. Freedman, and J. Tennyson, ExoMol molecular line lists XXXIX: Rovibrational molecular line list for CO$_2$, Mon. Not. R. Astron. Soc. **496**, 5282 (2020).

[23] H. Fleurbaey, R. Grilli, D. Mondelain, S. Kassi, A. Yachmenev, S. N. Yurchenko, and A. Campargue, Electric-quadrupole and magnetic-dipole contributions to the $\nu_2 + \nu_3$ band of carbon dioxide near 3.3 μm, J. Quant. Spectrosc. Radiat. Transfer (2021), submitted.

[24] O. I. Korablev, D. A. Belyaev, Y. S. Dobrolenskiy, A. Y. Trokhimovskiy, and Y. K. Kalinnikov, Acousto-optic tunable filter spectrometers in space missions (Invited), Appl. Optics **57**, C103 (2018).

[25] S. N. Yurchenko, W. Thiel, and P. Jensen, Theoretical ROVibrational Energies (TROVE): A robust numerical approach to the calculation of rovibrational energies for polyatomic molecules, J. Mol. Spectrosc. **245**, 126 (2007).

[26] A. Yachmenev and S. N. Yurchenko, Automatic differentiation method for numerical construction of the rotational-vibrational Hamiltonian as a power series in the curvilinear internal coordinates using the Eckart frame, J. Chem. Phys. **143**, 014105 (2015).

[27] S. N. Yurchenko, A. Yachmenev, and R. I. Ovsyannikov, Symmetry adapted ro-vibrational basis functions for variational nuclear motion: TROVE approach, J. Chem. Theory Comput. **13**, 4368 (2017).

[28] K. L. Chubb, A. Yachmenev, J. Tennyson, and S. N. Yurchenko, Treating linear molecule HCCH in calculations of rotation-vibration spectra, J. Chem. Phys. **149**, 014101 (2018).

[29] S. N. Yurchenko and T. M. Mellor, Treating linear molecule XY$_2$ in calculations of rotation-vibration spectra, J. Chem. Phys. , submitted (2020).

[30] X. Huang, D. W. Schwenke, R. S. Freedman, and T. J. Lee, Ames-2016 line lists for 13 isotopologues of co$_2$: Updates, consistency, and remaining issues, J. Quant. Spectrosc. Radiat. Transf. **203**, 224 (2017).

[31] I. E. Gordon and et al., The *HITRAN* 2016 molecular spectroscopic database, J. Quant. Spectrosc. Radiat. Transf. **203**, 3 (2017).

[32] T. Furtenbacher, A. G. Császár, and J. Tennyson, MARVEL: measured active rotational-vibrational energy levels, J. Mol. Spectrosc. **245**, 115 (2007).

[33] A. G. Császár, G. Czakó, T. Furtenbacher, and E. Mátyus, An active database approach to complete rotational–vibrational spectra of small molecules, Annu. Rep. Comput. Chem. **3**, 155 (2007).

[34] T. Furtenbacher and A. G. Császár, The role of intensities in determining characteristics of spectroscopic networks, J. Molec. Struct. (THEOCHEM) **1009**, 123 (2012).

[35] R. Tóbiás, T. Furtenbacher, J. Tennyson, and A. G. Császár, Accurate empirical rovibrational energies and transitions of H$_2^{16}$O, Phys. Chem. Chem. Phys. **21**, 3473 (2019).

[36] S. Mikhailenko, S. Tashkun, T. Putilova, E. Starikova, L. Daumont, A. Jenouvrier, S. Fally, M. Carleer, C. Hermans, and A. Vandaele, Critical evaluation of measured rotation–vibration transitions and an experimental dataset of energy levels of hd18o, J. Quant. Spectrosc. Radiat. Transf. **110**, 597 (2009), hITRAN.

[37] S. Tashkun, T. Velichko, and S. Mikhailenko, Critical evaluation of measured pure-rotation and rotation-vibration line positions and an experimental dataset of energy levels of 12C16O in X $^1\Sigma^+$ state, J. Quant. Spectrosc. Radiat. Transf. **111**, 1106 (2010), special Issue Dedicated to Laurence S. Rothman on the Occasion of his 70th Birthday.

[38] S. A. Tashkun, V. I. Perevalov, R. R. Gamache, and J. Lamouroux, CDSD-296, high resolution carbon dioxide spectroscopic databank: Version for atmospheric applications, J. Quant. Spectrosc. Radiat. Transf. **152**, 45 (2015).

[39] S. A. Tashkun, V. I. Perevalov, J. L. Teffo, L. S. Rothman, and V. Tyuterev, Global fitting of ^{12}c^{16}o$_2$ vibrational-rotational line positions using the effective hamiltonian approach, J. Quant. Spectrosc. Radiat. Transf. **60**, 785 (1998).

[40] A. Owens and A. Yachmenev, Richmol: A general variational approach for rovibrational molecular dynamics in external electric fields, J. Chem. Phys. **148**, 124102 (2018).

[41] A. Yachmenev, L. V. Thesing, and J. Küpper, Laser-induced dynamics of molecules with strong nuclear quadrupole coupling, The Journal of Chemical Physics **151**, 244118 (2019), arXiv:1910.13275 [physics].

[42] R. N. Zare, *Angular Momentum: Understanding Spatial Aspects in Chemistry and Physics*, 1st ed. (Wiley, 1988).

[43] T. H. Dunning, Gaussian basis sets for use in correlated molecular calculations. I. The atoms boron through neon and hydrogen , J. Chem. Phys. **90**, 1007 (1989).

[44] R. A. Kendall, T. H. Dunning, and R. J. Harrison, Electron affinities of the first-row atoms revisited. Systematic basis sets and wave functions, J. Chem. Phys. **96**, 6796 (1992).

[45] K. A. Peterson and T. H. Dunning, Accurate correlation consistent basis sets for molecular core–valence correlation effects: The second row atoms Al–Ar, and the first row atoms B–Ne revisited, J. Chem. Phys. **117**, 10548 (2002).

[46] G. E. Scuseria, Analytic evaluation of energy gradients for the singles and doubles coupled cluster method including perturbative triple excitations: Theory and applications to foof and cr2, J. Chem. Phys. **94**, 442 (1991), https://doi.org/10.1063/1.460359.

[47] J. Stanton, J. Gauss, M. Harding, and et al., (2019), cFOUR, a quantum chemical program package written by J.F. Stanton, J. Gauss, M.E. Harding, P.G. Szalay with contributions from A.A. Auer, R.J. Bartlett, U. Benedikt, C. Berger, D.E. Bernholdt, Y.J. Bomble, L. Cheng, O. Christiansen, M. Heckert, O. Heun, C. Huber, T.-C. Jagau, D. Jonsson, J. Jusélius, K. Klein, W.J. Lauderdale, D.A. Matthews, T. Metzroth, L.A. Mück, D.P. O'Neill, D.R. Price, E. Prochnow, C. Puzzarini, K. Ruud, F. Schiffmann, W. Schwalbach, S. Stopkowicz, A. Tajti, J. Vázquez, F. Wang, J.D. Watts and the integral packages MOLECULE (J. Almlöf and P.R. Taylor), PROPS (P.R. Taylor), ABACUS (T. Helgaker, H.J. Aa. Jensen, P. Jørgensen, and J. Olsen), and ECP routines by A. V. Mitin and C. van Wüllen. For the current version, see http://www.cfour.de.

[48] M. Battaglia, A. Buckingham, D. Neumark, R. Pierens, and J. Williams, The quadrupole moments of carbon dioxide and carbon disulphide, Mol. Phys. **43**, 1015 (1981).

[49] J. N. Watson, I. E. Craven, and G. L. Ritchie, Temper-

ature dependence of electric field-gradient induced bire-fringence in carbon dioxide and carbon disulfide, Chem. Phys. Lett. **274**, 1 (1997).

[50] N. Chetty and V. Couling, Measurement of the electric quadrupole moments of CO_2 and OCS, Mol. Phys. **109**, 655 (2011).

[51] H. Kling and W. Hüttner, The temperature dependence of the Cotton-Mouton effect of N_2, CO, N_2O, CO_2, OCS, and CS_2 in the gaseous state, Chem. Phys. **90**, 207 (1984).

[52] W. Ho, G. Birnbaum, and A. Rosenberg, Far-Infrared Collision-Induced Absorption in CO_2. I. Temperature Dependence, J. Chem. Phys. **55**, 1028 (1971), https://doi.org/10.1063/1.1676181.

[53] A. Hourri, J. M. St-Arnaud, and T. K. Bose, Dielectric and pressure virial coefficients of imperfect gases: CO_2-SF_6 mixtures, J. Chem. Phys. **106**, 1780 (1997), https://doi.org/10.1063/1.473317.

[54] S. Coriani, A. Halkier, A. Rizzo, and K. Ruud, On the molecular electric quadrupole moment and the electric-field-gradient-induced birefringence of CO_2 and CS_2, Chem. Phys. Lett. **326**, 269 (2000).

[55] G. Maroulis, Electric (hyper)polarizability derivatives for the symmetric stretching of carbon dioxide, Chem. Phys.

291, 81 (2003).

[56] A. Campargue, S. Kassi, A. Yachmenev, A. A. Kyuberis, J. Küpper, and S. N. Yurchenko, Observation of electric-quadrupole infrared transitions in water vapor, Phys. Rev. Research **2**, 023091 (2020).

[57] A. Campargue, A. M. Solodov, A. A. Solodov, A. Yachmenev, and S. N. Yurchenko, Detection of electric-quadrupole transitions in water vapour near 5.4 and 2.5 μm, Phys. Chem. Chem. Phys. **22**, 12476 (2020).

[58] T. Karman, M. A. J. Koenis, A. Banerjee, D. H. Parker, I. E. Gordon, A. van der Avoird, W. J. van der Zande, and G. C. Groenenboom, O_2-O_2 and O_2-N_2 collision-induced absorption mechanisms unravelled, Nature Chemistry **10**, 549 (2018).

[59] E. Rusak, J. Straubel, P. Gładysz, M. Göddel, A. Kedziorski, M. Kühn, F. Weigend, C. Rockstuhl, and K. Słowik, Enhancement of and interference among higher order multipole transitions in molecules near a plasmonic nanoantenna, Nature Communications **10**, 5775 (2019), arXiv:1905.08482 [physics.optics].

[60] J. Mun and J. Rho, Importance of higher-order multipole transitions on chiral nearfield interactions, Nanophotonics **8**, 46 (2019).